

Temperature stability of individual plasmonic Au and TiN nanodiscs: supplement

RYAN BOWER,^{1,*}  CILLIAN P. T. MCPOLIN,^{2,3,4} ALEXEY V. KRASAVIN,² ANATOLY V. ZAYATS,² AND PETER K. PETROV¹

¹*Department of Materials, Imperial College London, Royal School of Mines, Exhibition Road, London, SW7 2AZ, UK*

²*Department of Physics, King's College London, Strand, London, WC2R 2LS, UK*

³*Present address: Department of Chemistry, Molecular Sciences Research Hub, Imperial College London, White City, London W12 0BZ, UK*

⁴*c.mcpolin@imperial.ac.uk*

**r.bower16@imperial.ac.uk*

This supplement published with Optica Publishing Group on 9 August 2022 by The Authors under the terms of the [Creative Commons Attribution 4.0 License](https://creativecommons.org/licenses/by/4.0/) in the format provided by the authors and unedited. Further distribution of this work must maintain attribution to the author(s) and the published article's title, journal citation, and DOI.

Supplement DOI: <https://doi.org/10.6084/m9.figshare.20368767>

Parent Article DOI: <https://doi.org/10.1364/OME.462582>

Temperature stability of individual plasmonic Au and TiN nanodiscs: supplemental document

1. Fabrication methods

For both TiN and Au disc fabrication, all substrates were cleaned using standard solvent cleaning prior to resist coating. Following this, samples were exposed to an O₂ environment to ensure complete removal of solvent residues using a Diener Femto A plasma cleaner. PMMA resist was spin-coated onto the samples using a Luarell Model WS-650MZ-23NPP Spincoater, operating at 3,500 rpm, 2.000 rpm² acceleration for 1 minute. Following spin coating, samples were baked on a hotplate at 180 °C for three minutes. To improve write efficiency, a layer of the conductive polymer E-Spacer 300Z was spin-coated onto the surface of non-conductive samples (2,000 rpm, 1 minute) followed by a final bake at 90 °C for 90 s. Sample patterning was performed using a Raith™ E-Line EBL and SEM system with 20 keV beam, 10 μm aperture and 10 mm working distance.

Au disc fabrication

Gold discs were fabricated using an EBL lift-off method, as shown schematically in Fig. S1. Positive tone PMMA resist was directly applied to the bare Si (001) substrate. Disc arrays of varying diameter (150 nm to 450 nm) were written using electron beam lithography, and developed using MIBK:IPA (3:1). Following exposure and development, Au films were deposited onto the resist-patterned substrates via e-beam evaporation in a Mantis™ deposition system. Deposition parameters were 2 kV and 120 W, yielding a deposition rate of 0.2 Å s⁻¹. Prior to gold deposition, a Ti adhesion layer of ~5 nm was deposited onto the substrate via DC magnetron sputtering. Film thickness was measured using the in-situ QCM. Discs were revealed using acetone lift off.

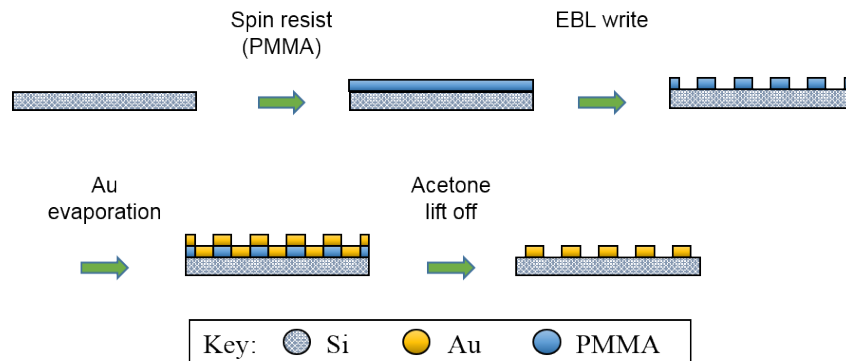


Fig. S1: Schematic of Au disc fabrication process.

TiN disc fabrication

Titanium nitride thin films were deposited using RF magnetron sputtering (Mantis™, 200 W, 600 °C) in which a Ti target (Pi-Kem, 99.99%) was sputtered in a 30% N₂:Ar reactive gas mixture. All films were deposited with a base chamber pressure of <math><5 \times 10^{-7}</math> mBar and a chamber residual oxygen pressure of <math><2.5 \times 10^{-9}</math> mBar.

Discs were patterned using a metallic Cr hard mask and chlorine based reactive ion etching. A positive EBL resist was applied to the TiN films, in this case PMMA, and discs were patterned using electron beam lithography. Following exposure and development (MIBK:IPA, 3:1) a 30 nm Cr hard mask was deposited via dc magnetron sputtering (Angstrom Amod) and lifted off in acetone.

The sample was then etched using a chlorine-based reactive ion etching method. A reactive gas mixture of BCl₃/Cl₂/Ar (5:8:15) was used yielding an etch rate of 100 nm min⁻¹. Following the TiN etch, the Cr masking layer was removed using chrome etchant. A schematic of the patterning process for TiN discs is included in Fig. S2.

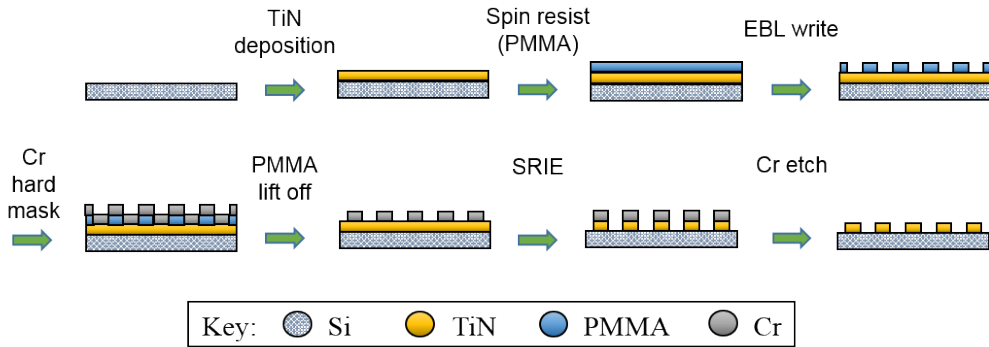


Fig. S2: Schematic of TiN disc fabrication process.

In both cases, spectroscopic ellipsometry and XRD data were collected for the thin films after deposition. A blank, un-patterned Si substrate was included and the structural and optical properties of the thin films were assessed prior to patterning. As demonstrated in Fig. S3, TiN films display single ENZ behavior and crystallinity with preferred orientation in the [002] direction. Au films also have optical properties comparable to literature values.

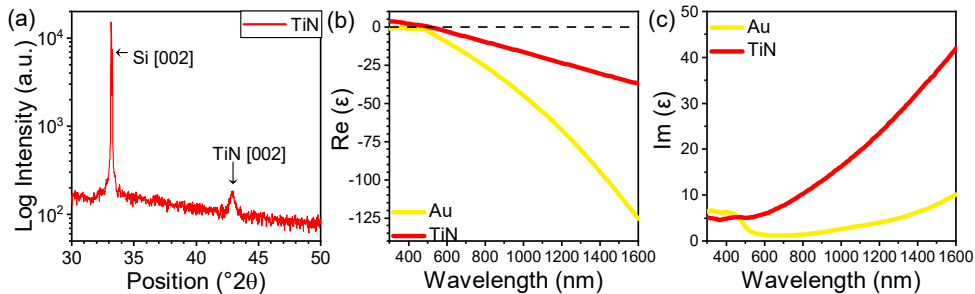


Fig. S3: (a) XRD data for TiN thin films. (b, c) Real (b) and imaginary (c) parts of permittivity of TiN and Au thin films, measured via spectroscopic ellipsometry.

2. Annealing studies

Annealing Study: 30 min anneal time

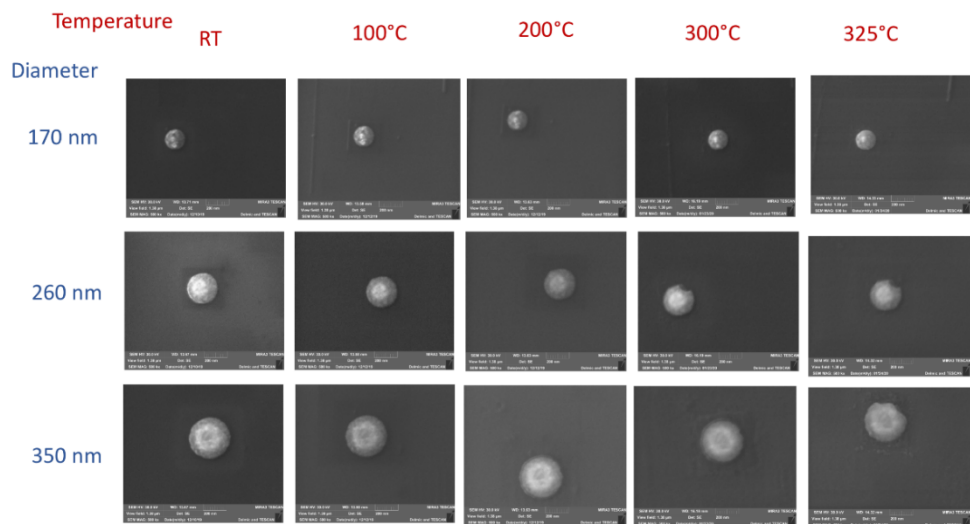


Fig. S4: SEM images of Au discs (170 nm, 260 nm, 350 nm) taken after each annealing step corresponding to Fig. 2.

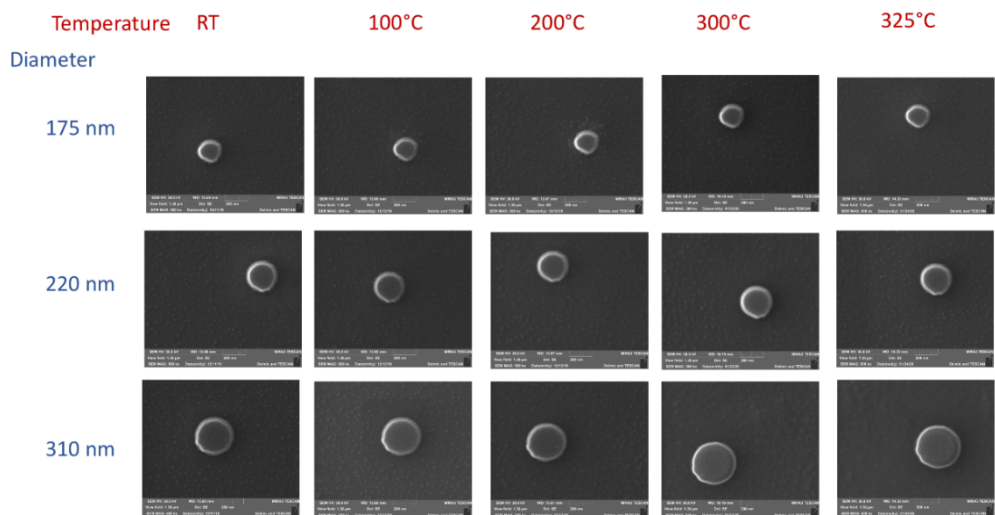


Fig. S5: SEM images of TiN discs (175 nm, 220 nm, 310 nm) taken after each annealing step corresponding to Fig. 2.

Annealing Study: 10 min anneal time

An additional annealing study was performed on TiN and Au samples for the same range of temperatures but a shorter anneal time of 10 min in order to compare to the previous study in Ref [1].

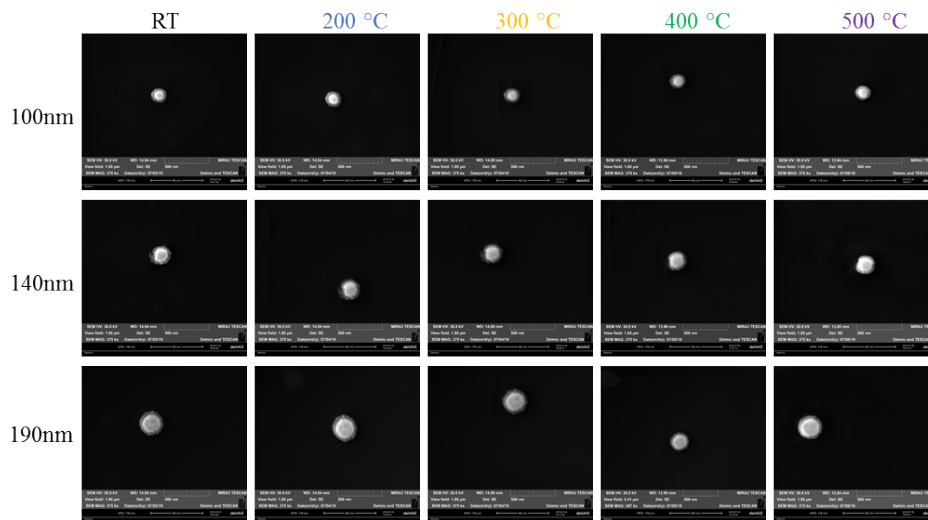


Fig. S6: SEM images for Au discs (100 nm, 140 nm, 190 nm) taken after each 10 min annealing step.

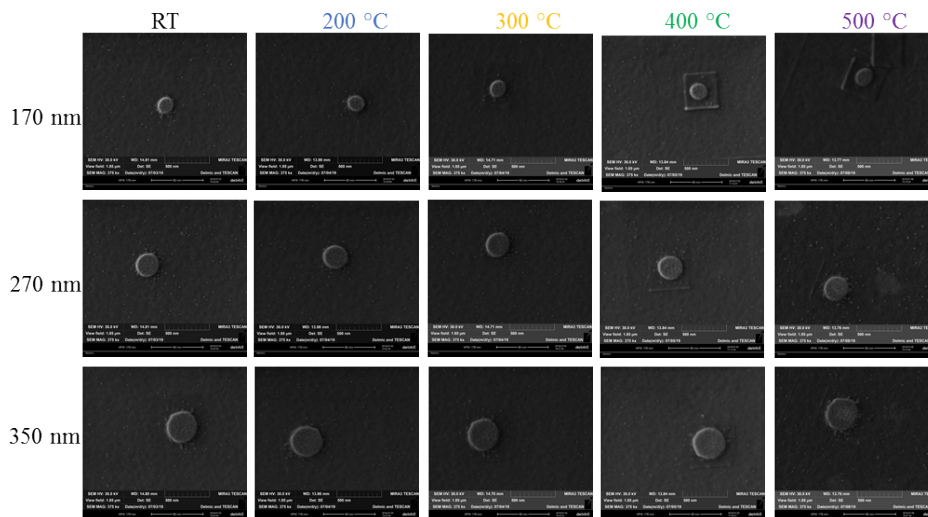


Fig. S7: SEM images of TiN discs (170 nm, 270 nm, 350 nm) taken after each 10 min annealing step.

SEM images show very small changes in the morphology of both Au (Fig. S6) and TiN (Fig. S7) discs, although slight softening of the Au edges is seen from 400 °C. Little variation in the optical response from Au discs was observed although significant degradation in the optical response of TiN is evident from 300 °C (Fig. S8).

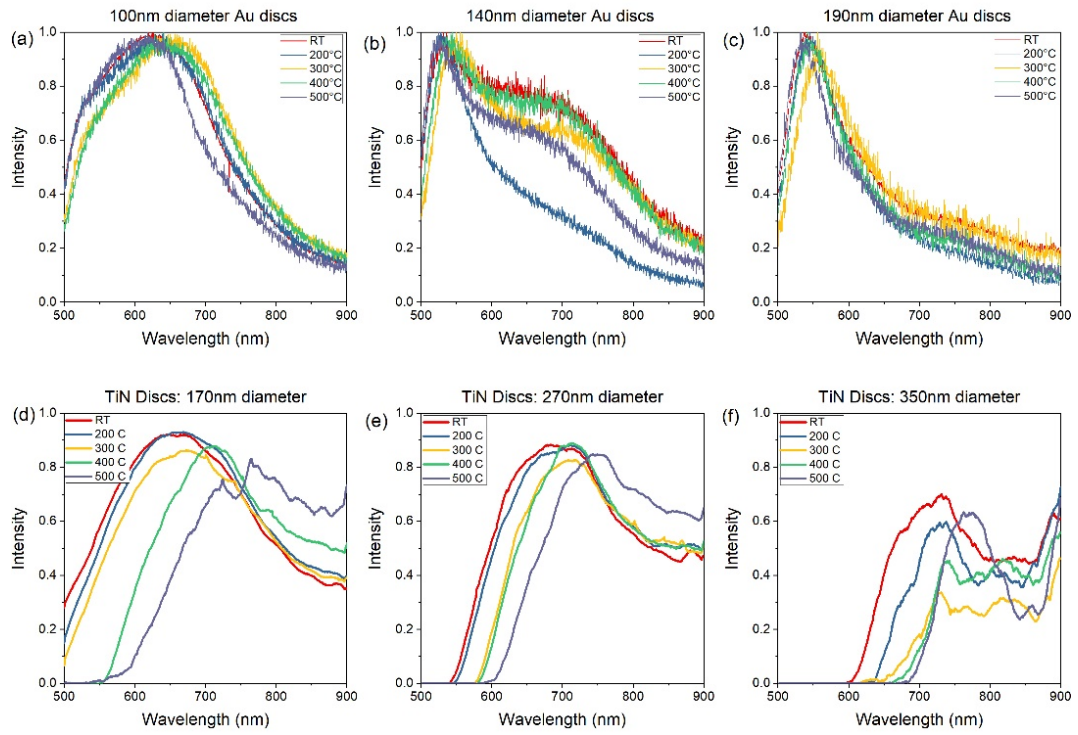


Fig. S8: Cathodoluminescence spectra from gold and titanium nitride discs corresponding to the annealing study in Fig. S6 and Fig. S7. Disk sizes and anneal temperatures are specified in the legends.

The apparent morphological stability of Au and the higher temperature required to initiate a change in optical response in TiN support the conclusion that a shorter annealing time will result in a higher attainable temperature before degradation occurs. This trend has also been noted previously in the case of TiN nanobowtie antennas [1] and TiN thin films [2].

Differences in the measured degradation temperature of TiN nanoparticles between this work and those reported in the literature may be related to the fact that in our work we measure the same nanoparticles, while other experiments measured an average response of the array which is not sensitive to small changes and, therefore, yielding higher temperatures for stable response.

3. Simulations

Resonance identification

To identify spectral features observed in the CL from the discs, numerical simulations were performed using plane wave illumination in a scattered field formulation. Au/Si and TiN nanodiscs of experimentally studied diameters placed on a Si substrate were illuminated at 45° by a plane wave with s -polarization to reveal in-plane plasmonic resonances of various orders and with p -polarization to additionally excite out-of-plane resonances (Fig. S7). The simulation domain was surrounded by perfectly matched layers to avoid back-reflection from the outer boundaries. The resonant frequencies were determined by the peaks in the extinction spectra, while resonances themselves were identified from the corresponding charge distributions. The optical properties of Au and Si were taken from [3] and [4] whereas for TiN experimentally collected ellipsometry data were used.

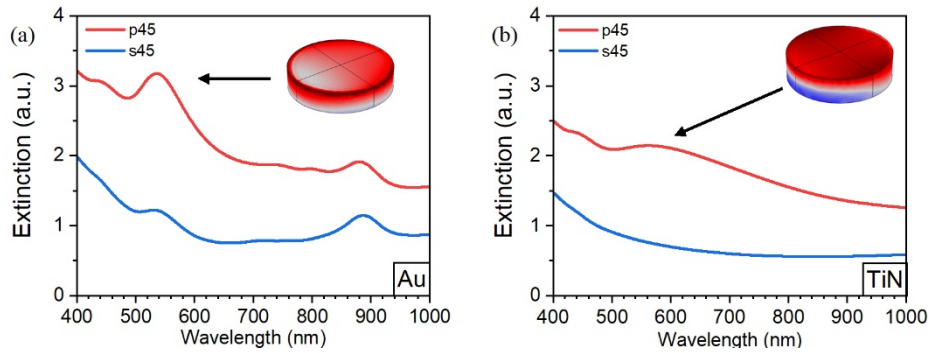


Fig. S9: Numerical simulations with plane wave excitation for both s - and p -polarizations at a 45° angle of incidence for (a) a Au disc with diameter 260 nm and (b) a TiN disc with diameter 220 nm. Insets show the charge distribution of the out-of-plane dipolar modes.

One can identify the plasmonic modes present in the simulated CL spectrum. Firstly, the high energy peak observed for both Au (at 540 nm) and TiN (at 580 nm) discs is attributed to an out-of-plane dipolar resonance and is pronounced only for p -polarization (Fig. S7, insets). Excitation of an out-of-plane dipolar resonance mode at similar wavelengths has previously been reported for Au discs measured via CL [5]. Secondly, the peak observed at approximately $\lambda=880$ nm in the simulated spectra for Au discs with $d=260$ nm is attributed to a higher order in-plane mode, specifically a quadrupolar mode, which is evident from its charge distribution. An in-plane dipolar mode will also be observed at longer wavelengths, red-shifting with increasing disc diameter. The simulated spectra for TiN discs show the presence of broader, lower energy resonances compared to the Au discs. This is due to the increased losses of TiN relative to Au. The simulated spectra above are in good agreement with the experimental CL spectra collected for both TiN and Au discs (Fig. 2) with the out of-plane dipolar resonance the dominant mode observed in the visible range for both materials.

CL modelling

Coherent cathodoluminescence is considered to be the dominant component of the CL signal for plasmonic nanostructures [6, 7] and was modelled by a point dipole positioned at the nanostructure interface where the electron beam hits the structure, representing a collapsing dipole produced by a moving electron and its mirror image. The top surface of the nanodisc was divided into five regions of equal areas (a circular central region and four consecutive rings around it) and CL signal from each area was simulated by placing the

dipolar source at the appropriate position (Fig. S8). The total CL signal is proportional to the sum of the obtained values.

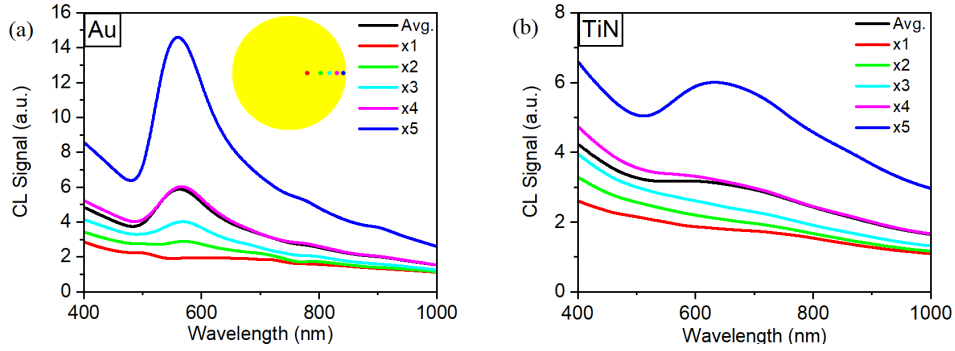


Fig. S10: Simulation of coherent CL response from varying positions, x , (see inset) along the disc radius for (a) a Au disc with diameter 260 nm and (b) a TiN disc with diameter 220 nm.

References

1. Gadalla, M.N., et al., *Excitation of Strong Localized Surface Plasmon Resonances in Highly Metallic Titanium Nitride Nano-Antennas for Stable Performance at Elevated Temperatures*. 2019.
2. Wells, M.P., et al., *Temperature stability of thin film refractory plasmonic materials*. Optics Express, 2018. **26**(12): p. 15726-15744.
3. Johnson P. B.; Christy, R.W., *Phys. Rev. B* **6**, 4370 (1972) - *Optical Constants of the Noble Metals*. 1972.
4. Schinke, C., et al., *Uncertainty analysis for the coefficient of band-to-band absorption of crystalline silicon*. AIP Advances, 2015. **5**(6): p. 067168.
5. Coenen, T., et al., *Directional emission from a single plasmonic scatterer*. Nature Communications, 2014. **5**(1): p. 3250.
6. P, C., et al., *Imaging of plasmonic modes of silver nanoparticles using high-resolution cathodoluminescence spectroscopy*. ACS nano, 2009. **3**(10).
7. Das, P. and T.K. Chini, *Spectroscopy and Imaging of Plasmonic Modes Over a Single Decahedron Gold Nanoparticle: A Combined Experimental and Numerical Study*. 2012.